Electronic structure of polychiral carbon nanotubes

Ph. Lambin,[1] V. Meunier,[2] and A. Rubio[3]
[1]*Département de Physique, FUNDP, 61 Rue de Bruxelles, B 5000 Namur, Belgium*
[2]*Department of Physics, North Carolina State University, Raleigh, North Carolina 27695*
[3]*Departamento Física Teórica, Universidad de Valladolid, E 47011 Valladolid, Spain*
and Donostia International Physics Center, San Sebastian, Spain
(Received 14 March 2000)

Most of the works devoted so far to the electronic band structure of multiwall nanotubes have been restricted to the case in which the individual layers have the same chirality. By comparison, much less is known on the electronic properties of multiwall nanotubes that mix different chiralities. These are interesting systems, however, since they can be composed of both metallic and semiconducting layers. For the present work, tight-binding calculations were undertaken for polychiral two-layer nanotubes such as (9,6)@(15,10), (6,6)@(18,2), and others. The recursion technique was used to investigate how the densities of states of the individual layers are affected by the intertube coupling. Constant-current scanning-tunneling-microscopy (STM) images were also calculated for these systems. The result obtained is that the image of a two-wall nanotube is pretty much the same as that of the isolated external layer. It is only in the case of monochiral, commensurate structures such as (5,5)@(10,10) that interlayer effects can be seen in the STM topography.

I. INTRODUCTION

Multiwall nanotubes (MWNT) have not attracted as much attention from theoreticians as single-wall carbon tubes did, although they may be useful in many applications. Multiwall nanotubes are obviously more complex than the one-layer tubules, which explains why the former are much less documented. As far as the electronic structure is concerned, calculations have already been performed for the simplest MWNT, those made of nonchiral layers .[1–7] The systems that were investigated in these works were all made of either zigzag or armchair nanotubes, without mixing. The reason was simply that mixing nanotubes with incommensurate periods along their axis leads to a nonperiodic system, which therefore precludes the use of the Bloch theorem and makes the calculations more difficult. However, there are many indications from electron diffraction[8–11] and scanning tunneling microscopy (STM) (Refs. 12 and 13) that the layers in a multiwall nanotube often have different chiralities with nearly random distribution.

The aim of the present paper is to investigate the electronic properties of polychiral nanotubes, namely multiwall structures mixing layers with different chiralities. The motivation of this work is twofold. First, we want to find out in which way electronic states can be induced in the band gap of a semiconducting layer by its coupling to a metallic tube of different chirality. The resulting interlayer coupling varies from site to site in a pseudorandom manner that could be responsible for localization of the electronic wave functions.[14,15] Indeed, a small concentration of pointlike defects in armchair nanotubes may induce a localization, as shown recently.[16] No such effects were detected in the present study where the interlayer interaction is a small, off-diagonal perturbation that affects all the sites. The second motivation was to see whether the electronic local density of states of the external layer of a MWNT can reflect the atomic structure of the underlying layers, leading to a pattern that could be observed with an STM. In some cases, MWNT analyzed with the STM appear like graphite, where only every other two atoms of the external layer are clearly imaged.[17,18] In other cases, there is a spatial modulation of the image intensity, most obviously because a perfect lattice coherence cannot be realized between two cylindrical graphitic sheets when the layers have different chiralities.[12] Our calculations show that, indeed, a site asymmetry of the STM image of a MWNT similar to that of graphite may appear, but this requires a special monochiral geometry like (5,5)@(10,10). In polychiral nanotubes, by contrast, there is no site asymmetry and no Moiré pattern in the STM images computed for bilayer systems. This conclusion is in agreement with recent STM images with atomic resolution obtained on MWNT,[13] although Moiré patterns have frequently been observed in other experiments as recalled here above.

All these effects were explored within a tight-binding description of the π electronic states, using the methodology presented in Sec. II. The results on the local DOS calculations for nanotubes mixing semiconducting and metallic layers are given in Secs. III and IV, and the STM image simulations are reported to Sec. V. All the calculations were restricted to bilayer nanotubes to keep the computing load reasonable.

II. METHODOLOGY

Several two-wall nanotubes were generated on the computer, with the requirement that the layer radii differ by approximately 0.34 nm, which corresponds to the observed interlayer distance in MWNT. In the π-electron tight-binding Hamiltonian used, the first-neighbor C pairs within a same layer received a $pp\pi$ hopping interaction $\gamma_0 = -2.75$ eV. This value was used for consistency with previous calculations of ours. That value slightly underestimates a recent experimental evaluation of γ_0 (-2.9 eV),[19] which simply means that our energies should be scaled by a factor 1.05.

This scaling does not alter any of the conclusions of the present work.

The interlayer interactions were written as $W\cos\phi\exp[-(d-\delta)/L]$ with d the distance between the coupled atoms, ϕ the angle between the π orbitals on these two atoms, $\delta=0.334$ nm, and $L=0.045$ nm. Two values of W were used to describe the graphite AA, BB, or AB-like interactions: $W=0.36$ eV for the first two and $W=0.16$ eV for the latter.[4] The range of the interlayer interactions was limited to a maximum distance $d=0.39$ nm. These parameters reproduce well first-principles calculations for MWNT.[2]

Local densities of states in the multiwall nanotubes were computed by the recursion method. This technique does not rely on the Bloch theorem. It gives rise to a continued-fraction expansion of the Green's-function diagonal elements in the complex energy plane, $G_{ii}(z)=\langle i|(z-H)^{-1}|i\rangle$. For each atomic site i of interest, $n=500$ levels of continued fraction were computed. This large number of levels is needed to properly sample the topology of the multiwall nanotube on a length of about 125 nm, and to obtain an energy resolution sufficient to observe the effects of the interlayer interactions. When the continued fraction is truncated after n levels, the resulting density of states is composed of n Dirac δ peaks. With $n-1$ levels, another set of $n-1$ peaks is obtained. These two interlaced sets were mixed with equal weights, and each δ peak was represented by a Gaussian function with standard deviation 0.023 eV (the bandwidth, $6|\gamma_0|$, divided by $\sqrt{2}n$). Due to this broadening, all the singularities of the densities of states, including the band edges, are slightly smoothed out. Due to its smallness, this broadening should not alter a main conclusion of the work, namely the absence of localized states in the gap of the semiconducting layer. The small Gaussian broadening used here avoids the need for a square-root termination of the continued fraction which does not work well in the presence of gaps or pseudogaps.

The change of density of states brought about by the interlayer coupling is expected to be small. The first-order perturbation expression of the Green function is indeed $G=G_0+G_0WG_0$. The unperturbed Green function G_0 is made of blocks corresponding to the individual layers that W couples together. Due to that structure, all the diagonal elements of G_0WG_0 are zero, which means that the density of states is not perturbed at first order in the interlayer interaction.

STM image simulations of multiwall nanotubes were performed for comparison with experiment. These calculations are based on a simple tight-binding theory of the STM current,[20]

$$I=(2\pi)^2\frac{e}{h}\int_{E_F^s-eV}^{E_F^s}dE\,n_t(E_F^t-E_F^s+eV+E)\times\sum_{i,i'\in s}v_{ti}v_{ti'}^{*}n_{ii'}^{s}(E),$$

where the E_F's are the Fermi levels of the tip (t) and sample (s) and V is the tip-sample bias potential. The tip is treated as a single atom with an s orbital and a Gaussian density of states $n_t(E)$. v_{ti} is the tight-binding hopping interaction between the tip atom and the π orbital located on site i of the nanotube sample, and $n_{ii'}^{s}(E)=(-1/\pi)\,\mathrm{Im}\,G_{ii'}^{s}(E)$. The Green-function elements $G_{ii'}$ of the nanotube were computed by recursion with 200 continued-fraction levels that give converged results for the present imaging studies. A small imaginary part was added to the energy to force the convergence.

TABLE I. Two-wall nanotubes with a metallic inner wall and a semiconducting outer wall. The second row is the interlayer distance, the third is the number of states induced in the gap (integrated DOS), and the fourth column is the standard deviation of the local density of states in the external layer (see Sec. V).

nanotube	R_2-R_1 (nm)	gap states/atom	rms (eV^{-1}/atom)
(6,6)@(19,0)	0.337	0.17×10^{-4}	3.7×10^{-4}
(6,6)@(18,2)	0.340	0.28×10^{-4}	2.4×10^{-4}
(10,−2)@(16,3)	0.337	0.56×10^{-4}	2.7×10^{-4}
(15,−6)@(15,10)	0.341	0.42×10^{-4}	3.2×10^{-4}
(9,6)@(15,10)	0.341	2.28×10^{-4}	2.8×10^{-4}

III. METAL-SEMICONDUCTOR NANOTUBES

We first consider two-wall nanotubes having a metal at the inner layer and a semiconductor at the outer layer. Table I gives a few such metal-semiconductor nanotubes. The first system mixes an armchair and a zigzag nanotube. Although these two nanotubes are nonchiral, their chiral angles differ by 30°, their translation periods differ by a factor of $\sqrt{3}$, and the combined system may be described as polychiral. The next three nanotubes of Table I are real polychiral systems. By contrast, the fifth nanotube is monochiral since its layers have the same chirality. This last nanotube differs from the fourth one by the fact that the inner layers (15,−6) and (9,6) are enantiomers. Hence, the two layers in the (15,−6)@(15,10) nanotube have the same Bravais period but have opposite chiral angles. In all the nanotubes, the position of the external layer with respect to the inner one was chosen at random. No structural optimization was performed.

The local density of states in the external layer was computed in a slice of 0.2 nm height, which contained between 32 and 40 atoms, depending on the nanotube. Although the coupling to the inner layer varies from site to site, all the atoms of the external layer were found to have pretty much the same density of states.

For all the polychiral nanotubes investigated, the density of states of the semiconducting layer was found to be weakly affected by its coupling to the inner metallic layer, at least in an interval between −1 and +1 eV (the zero of energy is always considered to be at the Fermi level). In that interval of energy, the metallic tube presents a constant density of states—hereafter called the metallic plateau—with no van Hove singularities. Figure 1(a), which concerns (15,−6)@(15,10), is a typical example of this effect. As compared to the single-wall (15,10) nanotube (dashed curve), there is a minute downshift of the bottom of the conduction band of the semiconducting layer (full curve), whereas the top of the valence band does not move. The shapes of the

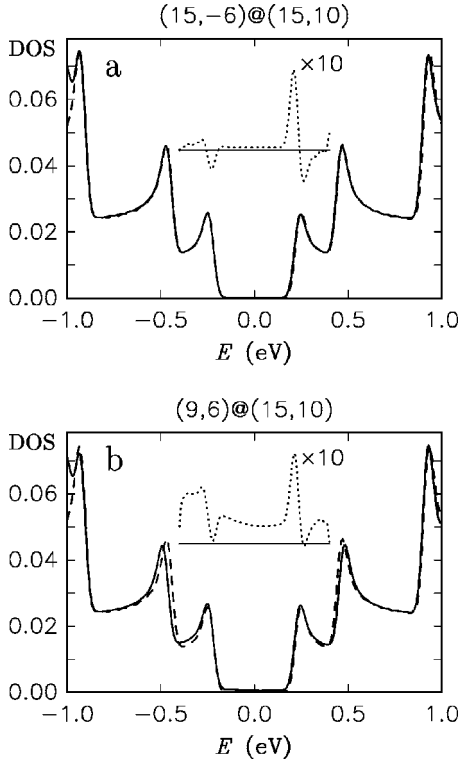

FIG. 1. Average density of states (eV^{-1}/atom) in the external layer of (a) (15,−6)@(15,10) and (b) (9,6)@(15,10) nanotubes (solid lines). The dashed curve is the density of states of the single-wall (15,10) nanotube. The differences between the DOS's of the two-layer and one-layer systems are shown by a dotted curve, displaced vertically for clarity (the horizontal bar indicates zero difference), and multiplied by a factor of 10.

gap edges are not modified. If the hopping interactions between the layers introduce a tailing of the valence and conduction states inside the gap, the decay will take place in an energy range shorter than the peak broadening used (0.023 eV). The metallic layer induces a few states in the band gap of the semiconductor (the total number of states in the band gap is 0.42×10^{-4} per atom of the semiconducting layer, see Table I). The density of states in the gap region is approximately uniform and very small (dotted curves).

The interlayer coupling is much more efficient in the monochiral (9,6)@(15,10) nanotube, as shown in Fig. 1(b). The density of states in the band-gap region is approximately five times larger than in Fig. 1(a) and reaches 2.5% of that of the metallic layer. Another indication that the interlayer coupling is efficient in this nanotube is the shift of the van Hove singularities which clearly appears by comparing the solid and dashed curves in Fig. 1(b), more especially in the occupied part of the DOS. It must be stressed that both nanotubes in Fig. 1 exhibit exactly the same electronic structure when the interlayer coupling is switched off. In other words, all the differences between the solid-line curves in Figs. 1(a) and 1(b) emerge from the different environments experienced by the (15,10) layer in both systems. The monochiral tubes constitute a particular case in which the electronic properties are much affected by specific symmetries in MWNT, both as pseudogaps in the local density of states or as a change in the intensity of every two atoms of the STM image (see below).

TABLE II. Same as Table I for polychiral two-wall nanotubes having a semiconducting inner wall and a metallic outer wall.

Nanotube	R_2-R_1 (nm)	gap states/atom	rms (eV^{-1}/atom)
(6,4)@(10,10)	0.337	2.4×10^{-4}	7.6×10^{-4}
(7,3)@(13,7)	0.340	2.2×10^{-4}	5.0×10^{-4}
(7,6)@(13,10)	0.341	2.1×10^{-4}	5.5×10^{-4}
(10,0)@(15,6)	0.342	2.6×10^{-4}	6.1×10^{-4}

A change of the width of the metallic plateau was also found in the case of commensurate three-wall armchair tubes.[21]

IV. SEMICONDUCTOR-METAL NANOTUBES

We now consider two-wall nanotubes having the semiconducting layer at the interior and the metallic layer outside. A list of such nanotubes which mix different chiralities is given in Table II. The local densities of states in the inner layer were computed in a slice of 0.3 nm height, which contained between 24 and 32 atoms depending on the nanotube. Here again, the fluctuations of the densities of states in the semiconducting layer, although twice as large as in Sec. III, remained small (see Table II). The local densities of states were then averaged as before.

The ratio between the band gap of the semiconductor and the width of the metallic plateau of the metal is now approximately 2:3, instead of 1:6 as for the previous configurations (Sec. III). For instance, the metallic plateau of the (10,10) nanotube is bounded by two Van Hove singularities at $E=\pm0.9$ eV. These singularities can be seen in the density of states of the (6,4) layer in the (6,4)@(10,10) bilayer [Fig. 2(a)]. In the conduction band, for instance, the singularity leads to a resonance followed by an antiresonance. This kind of structure was frequently observed among the nanotubes of Table II. In a systematic way, also, the band gap of the semiconductor is reduced by the coupling to the outer layer: the top of the valence band has moved upwards by approximately 0.03 eV.

As shown in Fig. 2(a), the density of states in the band gap of the inner semiconducting tube is small, but still significantly higher than in Fig. 1(a), for instance. The difference between these two situations is that the semiconducting layer is now at the interior rather than at the exterior, and the inner layer is more perturbed than the outer one. Indeed, the average numbers of intersheet bonds per atom in layers 1 and 2 are inversely proportional to the number of atoms in these layers. Since there are approximately two times fewer atoms in the inner layer than in the outer (for those systems we are investigating), the interlayer coupling is two times more efficient on layer 1 than on layer 2. Since, in addition, the (6,4) semiconductor has a larger band gap than those of the semiconducting layers of Table I (due to its smaller diameter), the number of states in the gap has increased. As revealed by Table II, the number of states in the gap looks remarkably constant for all the nanotubes examined, around 2.3×10^{-4} per atom.

As for the metallic layer, one can hardly see any change in its density of states around the Fermi level [Fig. 2(b)]. The site-to-site fluctuations of densities of states near the Fermi level are less than 1% of the (10,10) density of states at E_F.

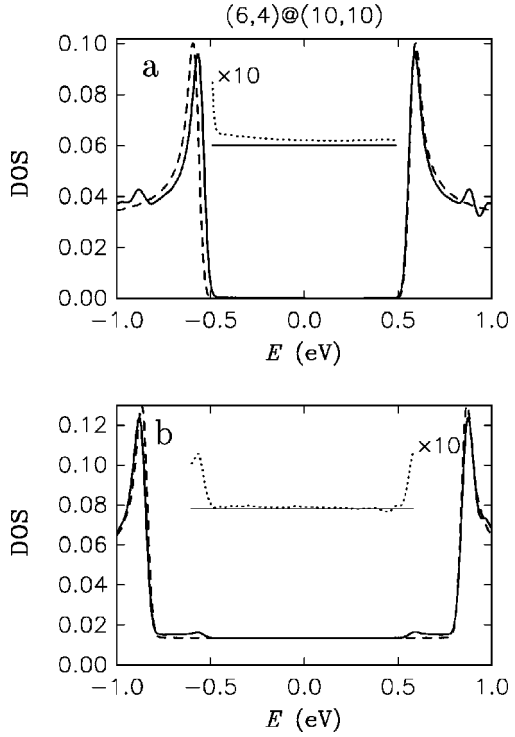

FIG. 2. Average density of states in (a) the inner and (b) the outer layer of (6,4)@(10,10) (solid lines). The dashed curves in (a) and (b) show the density of states of the isolated (6,4) and (10,10) nanotubes. The differences between the solid and dashed curves are shown by the dotted curves after amplification by a factor of 10.

This kind of weak disorder, here due to the coupling with a chiral nanotube, is small but is perhaps sufficient to affect the transport properties of a MWNT in the weak-localization regime.[22,23] Clear effects of the coupling to the inner layer appear below -0.5 eV and above $+0.5$ eV, where the (6,4) nanotube has its band edges. It is clear from this example that the amplitudes of the Van Hove singularities at $E=\pm 0.9$ eV are reduced as compared with the single-wall nanotube. This is due to the breaking of the translational symmetry brought about by the coupling between layers of different chiralities.

V. SIMULATION OF THE STM IMAGE OF TWO-WALL NANOTUBES

Several constant-current STM images of multiwall nanotubes show intensity or contrast modulations.[12,18] Such modulations have been interpreted as being a Moiré pattern formed by the atomic structure of the last two layers. In graphite, Moiré pattern effects have clearly been identified with an STM in regions where the last layer was folded back on the surface with a misorientation of its crystallographic directions.[24]

As pointed out in the previous sections, the local DOS shows only little variations on going from one site to another in a multiwall nanotube. To quantify that property, the fluctuations (rms) of the local DOS were computed on a chain of 25 first-neighbor atoms located as close as possible to a generator of the external layer. These atoms were selected because they would be probed in a scan of the topmost part of the nanotube by a STM tip. The DOS fluctuations, averaged

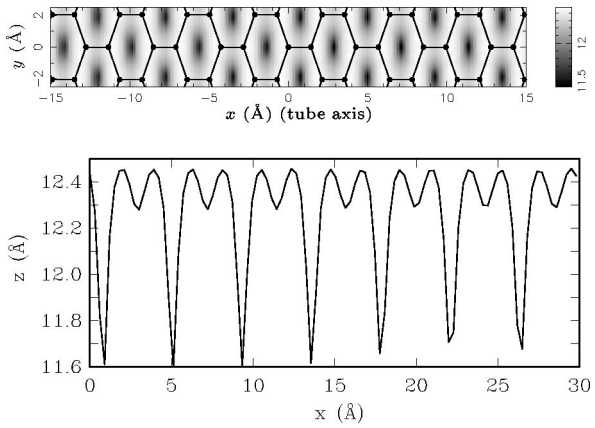

FIG. 3. Top: computed constant-current image of the topmost part of the (6,6)@(19,0) two-layer nanotube. The nanotube axis is parallel to the horizontal x direction. The tip potential is 0.5 V, the height of the tip above the atom at the origin of the x,y coordinates is 5 Å (all the coordinates are in Å). Bottom: topographic line cut across the image, along the $y=0$ line.

over the energy interval $(-1,+1)$ eV, are listed in the last row of Tables I and II. They are small, less than 1% of the mean density of states. According to these data, the spatial variations of the density of states in polychiral nanotubes cannot explain the modulations of the STM image intensity.

Figure 3 is a simulation of the STM image of (6,6)@(19,0) computed with the methodology described in Sec. II. The tip is at a potential of 0.5 V with respect to the sample. For that polarity, the most prominent features in the STM image of the semiconducting (19,0) layer are the CC bonds not parallel to the axis, which appear as bright stripes at 60° to the axis.[25] All along the portion of nanotube displayed, the periodicity of the image is that ($\sqrt{3}a$, with a the lattice parameter of graphene) of the external zigzag layer. There is no visible sign of the underlying armchair nanotube with its shorter period a. The topographic line cut shown at the bottom of Fig. 3 clearly proves that statement. The sharp minima of the curve correspond to the centers of the hexagons. The apparent variations of their depth are due to the pixel discretization. The maxima correspond to the atoms; the secondary minima are at the center of the CC bonds parallel to the axis.

Nothing similar to a Moiré pattern appears in the computed STM image of Fig. 3 nor in the simulations we carried out for other polychiral nanotubes. However, these patterns occur occasionally in the experimental images of multiwall nanotubes, as reported above. It is not impossible that a mechanical deformation of the outer layer of the tube caused by the STM tip induces metallic islands (with a much larger density of states) at special places where the layers are in suitable registry. The pressure of the tip may also induce better electric contact with the substrate at some places, leading to a larger tunneling current. Intrinsic defects of the nanotubes, such as a deviation from the coaxial geometry, some polygonization of the cross section, or a nonuniform twist along the axis, may be other possible causes for the observation of a Moiré pattern.

The atoms in Fig. 3 all look the same, unlike the case of multilayer graphite where the STM current at low bias (~ 0.1 V) shows a strong site asymmetry.[26] This asymmetry

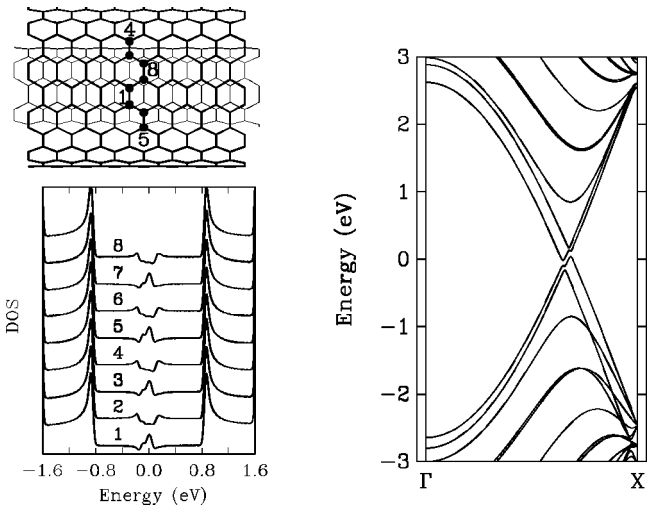

FIG. 4. π-electron band structure of (5,5)@(10,10) and local density of states on the sites labeled 1–8 in the external layer. The configuration of the nanotube, with symmetry C_{5h}, is sketched in the top-left part. The unit cell of the (10,10) tube can be obtained from the eight atoms represented by the black dots by application of $2\pi/5$ rotations about the axis.

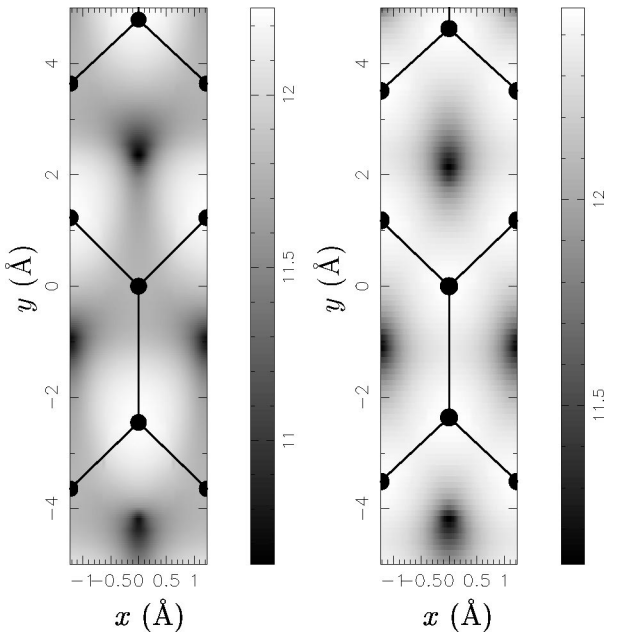

FIG. 5. Gray-scale representation of the radial distance $\rho(x,y)$ at constant current of the STM tip apex above a short azimuthal portion of (5,5)@(10,10) (left) and (6,6)@(11,11) (right). The orientation of the two layers in (5,5)@(10,10) is the C_{5h} configuration of Fig. 4. The tube axes are along the horizontal direction and the tip potential is fixed at 0.1 V.

is already present with two layers only,[21] since the coupling makes the atoms having a neighbor underneath different from those that have not (A and B atoms, respectively).

In a multiwall nanotube, it is impossible to realize the same stacking as in natural graphite all around the cross section. However, at least one multiwall nanotube exists where the topographic STM image is predicted to look like that of graphite. This case is (5,5)@(10,10).[21] This system is known to exhibit small pseudogaps near E_F as the consequence of avoided band crossings[6] for relative tube orientations such that the mirror planes of (5,5) do not coincide with those of (10,10).[3] Local DOS calculations then show that the atoms (of the external layer) are not equivalent, at least in a small interval around the Fermi level. Interestingly, first-neighbor atoms have a peak or a valley at E_F, alternatively, very much like in graphite, where the A and B atoms alternate. This effect is shown in Fig. 4. The explanation of this bipartition of the honeycomb lattice is presented in the Appendix. A consequence of it is that the STM image of the (5,5)@(10,10) nanotube at low bias resembles that of graphite, with maxima of protrusion on every other two atoms (those with the largest DOS at E_F), see Fig. 5. However, for other relative orientations of the tubes, no bipartition effect is observed (in agreement with first-principles calculations[7,21]). What is special about (5,5)@(10,10) is that this system has at least a fivefold common symmetry. In (6,6)@(11,11), for instance, there is no axial symmetry, which destroys the effects of the interlayer coupling on the DOS around the Fermi level, very much like in polychiral nanotubes. The resulting intertube interaction averaging reduces any symmetry-related feature such as the opening of pseudogaps and the bipartition of the honeycomb lattice. The STM image of (6,6)@(11,11) is then similar to that of the isolated single-wall (11,11) nanotube (see Fig. 5). With other metallic nanotubes such as (7,4)@(12,9), which we also have examined, some variations of the local DOS from one atom to the other were detected in the metallic plateau, but these were two small to lead to a clear site asymmetry in the STM image.

The property that (5,5)@(10,10) presents a site asymmetry that depends on the relative orientation of the layers can be illustrated by giving a uniform torsion to the (10,10) nanotube. At regular intervals along the axis, the planes that bisect the CC bonds perpendicular to the axis of (10,10) coincide with the mirror planes of (5,5) (C_{5v} symmetry, no site asymmetry). Away from these positions, the local symmetry of the atomic structure is lower and the two-site asymmetry of the DOS should come out and reach a maximum in between.

The twist is equivalent to applying a shear of the honeycomb network, which affects the bond lengths and opens a small gap at the Fermi level.[27,28] The calculations were performed for a twist of 1.5° (shear strain) corresponding to a torsion angle of 2.2°/nm, which leads to a band gap of 0.25 eV (the γ_0 parameter was scaled according to a d^{-2} law, with d the bond length). In the (5,5)@(10,10) distorted nanotube, the local DOS of the twisted (10,10) layer has a peak near the Fermi energy induced by the interactions with the inner (5,5) nanotube [Fig. 6(b)]. The shear also affects the Brillouin zone of the rolled-up graphene sheet, which moves the Fermi points of the twisted (10,10) nanotube away from those of the (5,5) layer. As a consequence, the minigaps of the bilayer are no longer located at the center of the metallic plateau (where the semiconducting gap of the twisted nanotube has opened) but are shifted 0.25 eV on both sides of the Fermi level. As can be seen in Fig. 6(a), the DOS features in the minigaps at ± 0.25 eV resemble the two-site asymmetry observed near E_F in Fig. 4 for the perfect (5,5)@(10,10), except that the magnitude of the asymmetry now varies along the tube. The DOS curves in Fig. 6(a) correspond to 25 successive atoms along a longitudinal zigzag chain on the

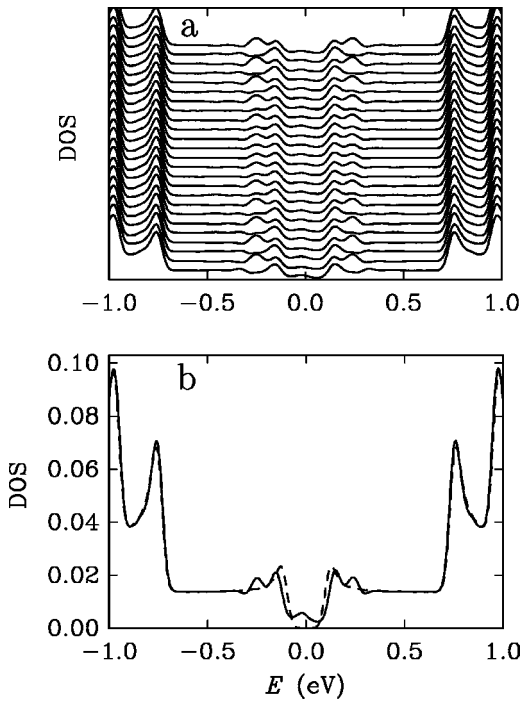

FIG. 6. Local DOS in the outer layer of (5,5)@(10,10) obtained by twisting the (10,10) nanotube with a uniform torsion equal to 2.2°/nm. (a) Variations of the local DOS along a chain of 25 atoms located as close as possible to a generator of the external tube. (b) The average of the 25 curves shown in (a) (solid line) is compared to the DOS of the isolated twisted (10,10) nanotube (dashed curve).

external tube. The curves at the center all look the same, where the local symmetry of the (5,5)@(10,10) distorted nanotube is close to C_{5v}. By contrast, the curves at the bottom and at the top have peaks and valleys at $E=\pm 0.25$ eV that alternate from one site to the next. The local symmetry has been changed to C_5 in these regions. The modulation of the degree of inequivalence between the atoms is due to the continuous change of the local symmetry along the nanotube axis. Unfortunately, this modulation did not appear clearly in the STM images that we computed for bias potentials of -0.3 and $+0.3$ V. The reason is that the expression of the STM current (Sec. II) is an integral of the Green's-function elements over the bias window, to which the site-dependent features in the density of states in Fig. 6(a) contribute little. However, these features might be observable by current imaging tunneling spectroscopy.

VI. CONCLUSION

Two-wall nanotubes mixing metallic and semiconducting layers retain the basic properties of the uncoupled constituents, as shown previously for monochiral nanotubes.[1] The intertube interactions induce a small continuous distribution of states in the band gap of the semiconducting layer. The electronic states near the Fermi level come from the metallic tube and they will dominate the transport properties at low voltage in the weak localization regime. Constant-current STM images computed for polychiral nanotubes are pretty much the same as the ones obtained on the isolated external layer. It is only in the case of monochiral and commensurate structures like (5,5)@(10,10) that interlayer effects can be seen in the STM topography. The interlayer coupling gives rise to a site asymmetry in the STM image at low voltage (~ 0.1 V), similar to that obtained on multilayer graphite. This site bipartition is maximum when the symmetry of the two-wall nanotube is reduced to C_5, and it disappears when the symmetry is higher. The site asymmetry also disappears in rotationally incommensurate nanotubes like (6,6)@(11,11). In polychiral nanotubes, there is no site asymmetry and no Moiré patterns appear in the computed STM images. From the few cases we have investigated, it can be concluded that the superstructures often observed in the STM images of MWNT cannot be ascribed to pure electronic effects.

ACKNOWLEDGMENTS

This work has been partly funded by the interuniversity research project on reduced dimensionality systems (PAI P4/10) of the Belgian Office for Scientific, Cultural and Technical affairs, the EU NAMITECH contract ERBFMRX-CT96-0067 (DG12-MITH), and by a JCyL (Grant VA28/99). The authors acknowledge Laszlo P. Biró for helpful discussions.

APPENDIX: MULTIWALL ARMCHAIR NANOTUBES

In a single-wall armchair nanotube, the two bands that cross each other at the Fermi level correspond to the irreducible representation A_1 and A_2 of the symmetry group C_{5v} of the wave function for a general Bloch wave vector k. These wave functions are, respectively, symmetric and antisymmetric upon a reflection of the ''vertical'' mirror planes that bisect the CC bonds perpendicular to the nanotube axis. When all curvature effects are neglected in the Hamiltonian as here, the Fermi wave vector is independent of the tube diameter. This means that in a two-wall nanotube such as (5,5)@(10,10), the states at the Fermi points have a fourfold degeneracy when the interlayer coupling is ignored. In the presence of the coupling, the wave functions adapted to the perturbation W are linear combinations of the four Fermi states ψ_1^i, ψ_2^i, ψ_1^e, and ψ_2^e of the internal and external layers (upper indices i and e) corresponding to A_1 and A_2 symmetries (lower indices 1 and 2). These combinations of states diagonalize the perturbation matrix

$$\begin{pmatrix} 0 & 0 & w_{11}^{ie} & w_{12}^{ie} \\ 0 & 0 & w_{21}^{ie} & w_{22}^{ie} \\ w_{11}^{ei} & w_{12}^{ei} & 0 & 0 \\ w_{21}^{ei} & w_{22}^{ei} & 0 & 0 \end{pmatrix},$$

where $w_{12}^{ie}=\langle \psi_1^i|W|\psi_2^e\rangle$, etc. In any case, the perturbation is sufficient to split off the degeneracy of the Fermi states. In general, also, the eigenvector of the perturbation matrix will mix the four Fermi states. This means in particular that the perturbed wave functions at the Fermi level mix the ψ_1^e and ψ_2^e states of the external layer. By mixing these states, which are, respectively, even and odd with respect to the center of each CC bond, one forms a disymmetric combination. As a

result, there are now two kinds of unequivalent atoms in each layer, as shown by the density of states in Fig. 4, which explains the site asymmetry of the computed STM images.

An exception to this explanation arises when the four matrix elements of the kind w_{12}^{ie} along the ascending diagonal vanish for symmetry reasons. This takes place when the symmetry of the two-wall nanotube preserves the mirror planes of the inner layer. Then, A_1 and A_2 remain valid irreducible representations of the symmetry group of the coupled system, band crossings remain allowed, and there is no pseudogap formation in the density of states. This also means that the site asymmetry of the STM image disappears. For the (5,5)@(10,10) nanotube, this happens with C_{5v}, D_{5h}, and D_{5d} configurations of the layers.[3,4,6] The latter configuration corresponds to the minimum of the total energy of the nanotube.[2,6]

In the case where the two nanotubes have no axial symmetry in common, such as, for instance, with (6,6)@(11,11), all band crossings are avoided and two kinds of unequivalent atoms are formed in each layer, as above. However, due to a cancellation effect, all the elements in the perturbation matrix are found to be small except the ones derived from the totally symmetric states, w_{11}^{ie} and w_{11}^{ei}. In practice, then, all the atoms look equivalent. Also, the pseudogaps near the Fermi level are much weaker than for the (5,5)@(10,10) case.[4]

[1] R. Saito, G. Dresselhaus, and M.S. Dresselhaus, J. Appl. Phys. **73**, 494 (1993).
[2] J.C. Charlier and J.P. Michenaud, Phys. Rev. Lett. **70**, 1858 (1993).
[3] Ph. Lambin, L. Philippe, J.C. Charlier, and J.P. Michenaud, Comput. Mater. Sci. **2**, 350 (1994).
[4] Ph. Lambin, J.C. Charlier, and J.P. Michenaud, in *Progress in Fullerene Research*, edited by H. Kuzmany, J. Fink, M. Mehring, and S. Roth (World Scientific, Singapore, 1994), pp. 130–134.
[5] D. Östling, D. Tománek, and A. Rosén, Phys. Rev. B **55**, 13 980 (1997).
[6] Y. K. Kwon and D. Tománek, Phys. Rev. B **58**, R16 001 (1998).
[7] A. Rubio, Appl. Phys. A: Mater. Sci. Process. **68**, 275 (1999).
[8] S. Iijima, Nature (London) **354**, 56 (1991).
[9] X.F. Zhang, X.B. Zhang, G. Van Tendeloo, S. Amelinckx, M. Op de Beeck, and J. Van Landuyt, J. Cryst. Growth **130**, 368 (1993).
[10] M. Liu and J.M. Cowley, Carbon **32**, 393 (1994).
[11] S. Iijima, MRS Bull. 43 (1994).
[12] M. Ge and K. Sattler, Science **260**, 515 (1993).
[13] A. Hassanien, M. Tokumoto, S. Ohshima, Y. Kuriki, F. Ikazaki, K. Uchida, and M. Yumara, Appl. Phys. Lett. **75**, 2755 (1999).
[14] P.W. Anderson, Phys. Rev. **109**, 1492 (1958).
[15] P.A. Lee and T.V. Ramakrishnan, Rev. Mod. Phys. **57**, 287 (1985), and references therein.
[16] T. Kostyrko, M. Bartkowiak, and G.D. Mahan, Phys. Rev. B **60**, 10 735 (1999).
[17] N. Lin, J. Ding, S. Yang, and N. Cue, Carbon **34**, 1295 (1996).
[18] L.P. Biró, J. Gyulai, Ph. Lambin, J. B. Nagy, S. Lazarescu, G.I. Márk, A. Fonseca, P.R. Surján, Zs. Szekeres, P.A. Thiry, and A.A. Lucas, Carbon **36**, 689 (1998).
[19] R. Saito, G. Dresselhaus, and M. S. Dresselhaus, Phys. Rev. B **61**, 2981 (2000).
[20] V. Meunier and Ph. Lambin, Phys. Rev. Lett. **81**, 5588 (1998).
[21] Ph. Lambin, V. Meunier, and A. Rubio, in *Science and Applications of Carbon Nanotubes*, edited by D. Tománek and R.J. Enbody (Kluwer Academic Publisher, New York, 2000), pp. 17–34.
[22] L. Langer, V. Bayot, E. Grivei, J.P. Issi, J.P. Heremans, C.H. Olk, L. Stockman, C. Van Haesendonck, and Y. Bruynseraede, Phys. Rev. Lett. **76**, 479 (1996).
[23] X. Schönenberger, A. Bachtold, C. Strunk, J.P. Salvetat, and L. Forró, Appl. Phys. A: Mater. Sci. Process. **69**, 283 (1999).
[24] H. Beyer, M. Müller, and Th. Schimmel, Appl. Phys. A: Mater. Sci. Process. **68**, 163 (1999).
[25] C.L. Kane and E.J. Mele, Phys. Rev. B **59**, R12 759 (1999).
[26] D. Tománek and S.G. Louie, Phys. Rev. B **37**, 8327 (1988).
[27] A. Rochefort, Ph. Avouris, F. Lesage, and D.R. Salahub, Phys. Rev. B **60**, 13 824 (1999).
[28] L. Yang, M.P. Anantram, J. Han, and J.P. Lu, Phys. Rev. B **60**, 13 874 (1999).